UNIVERSITY of CALIFORNIA
SANTA CRUZ

ENERGY LOSS OF PROTONS IN SILICON STRIP DETECTORS FOR COMPUTED TOMOGRAPHY

A thesis submitted in partial satisfaction of the
requirements for the degree of

BACHELOR OF SCIENCE

in

PHYSICS

by

Carlin Fuerst

June 2010

The thesis of Carlin Fuerst is approved by:

Professor Hartmut Sadrozinski
Technical Advisor

Professor David P. Belanger
Thesis Advisor

Professor David P. Belanger
Chair, Department of Physics

Abstract

Energy Loss of Protons in Silicon Strip Detectors for Computed Tomography

by

Carlin Fuerst

The purpose of this paper is to analyze the effectiveness of a prototype instrument with applications in medical imaging. Radiobiologists at Loma Linda University Medical Center currently employ X-ray computed tomography as an imaging solution for their proton therapy patients. Researchers at the Santa Cruz Institute for Particle Physics have been commissioned to design and implement a prototype imaging solution that uses protons from the treatment beam instead of X-rays. This paper analyzes the energy loss of the particles as they pass through the tracking detectors before they reach the calorimeter which will aid engineers in creating a final product. Our preliminary results indicate that the GLAST 2000 detectors and electronics show us higher than expected calculated energy absorption values, specifically differences of 121%, 129%, and 87% from the expected values for 35MeV, 100MeV, and 250MeV beam energies.

Contents

List of Figures

List of Tables

To my loving parents,

Peter and Lorrie Fuerst,

who have always been there for me.

Acknowledgements

I would like to thank my friend and colleague Brian Colby without whose patience and clarity the time until my graduation would extend asymptotically and Ford Hurley for allowing himself to be muddled by my cryptic coding skills. I would also like to thank my advisor Hartmut Sadrozinski for putting his trust in my abilities long enough for me to do something worthwhile.

1 Introduction

Doctors at Loma Linda University Medical Center (LLUMC) currently employ a proton accelerator to generate a beam of high-energy protons for the purpose of treating cancerous tumors. The benefit of this form of radiation therapy is the ability to treat localized, isolated, solid tumors before they spread to other tissues and to the rest of the body[1]. While the treatment uses protons, X-ray Computed Axial Tomography (CAT) is currently used to generate three dimensional images of the patients' tumors. The drawbacks of this combination of proton treatment and X-ray imaging are that the instrumentation for both exist in separate rooms due to the size of the apparatus which requires the patient to be moved around and that the fundamental differences between the ways in which protons and photons interact with matter may limit the physical insight that we glean from the images. As a solution, engineers at the Santa Cruz Institute for Particle Physics (SCIPP) have been commissioned by LLUMC to develop the hardware for a Proton Computed Tomography (pCT) system that uses protons from the accelerator to image cancer patients. This is currently being done with Silicon Strip Detectors (SSDs) and custom readout electronics that were originally designed for the Gamma-ray Large Area Space Telescope (GLAST) aka Fermi for which SCIPP was a contributing research group. This paper will describe the progress of hardware development and analysis of the energy loss of protons through the tracking SSDs before they are inevitably measured by the calorimeter and the implications of this on the eventual imaging solution[2].

1.1 Characteristics of Proton Therapy

Using high-energy protons for radiation oncology was first proposed in 1946 and since then, several hospitals around the world have built proton accelerators for this purpose[1]. In the accelerator, hydrogen atoms are stripped of their electrons and sent through a vacuum tube within a pre-accelerator. At this point, the protons have each gained 2MeV in kinetic energy before entering the synchrotron where they travel around the loop 10 million times per second, gaining energy every trip from a radio frequency cavity in the loop. By the time the protons leave the accelerator, they have an energy between 70 and 250MeV. It is the nature of charged particles at these energies to penetrate matter while depositing a fraction of their energy via the excitation of electrons in the material. This interaction is described by the Bethe-Bloch formula which gives the mean stopping power of a material as a function of particle energy. In this model and range of energies, higher energy particles deposit less energy-per-distance penetrated than lower energy particles. This results in the particles depositing most of their energy deep inside a material, as opposed to near the surface as with X-rays, and this energy loss is characterized by what is called a Bragg peak. With a range of proton energies and a rotating beam aperture, the dose can be localized in a discrete volume within the patient resulting in a lower amount of collateral healthy tissue damage than X-ray therapy.

1.2 Description of pCT

The system currently in development at SCIPP through collaboration with LLUMC called pCT will provide doctors with an imaging solution that utilizes protons originally intended for radiation therapy which would simplify and potentially improve the process of treatment. The pCT system would contain as few as three main detectors for the purpose of particle tracking: Two tracking SSDs to record the X and Y positions of incident particles and a CsI calorimeter to measure the energy of said particles. The position trackers also have the ability to measure charge deposited in the detector in the form of TOT, or time over threshold, by converting the signal of the charge in

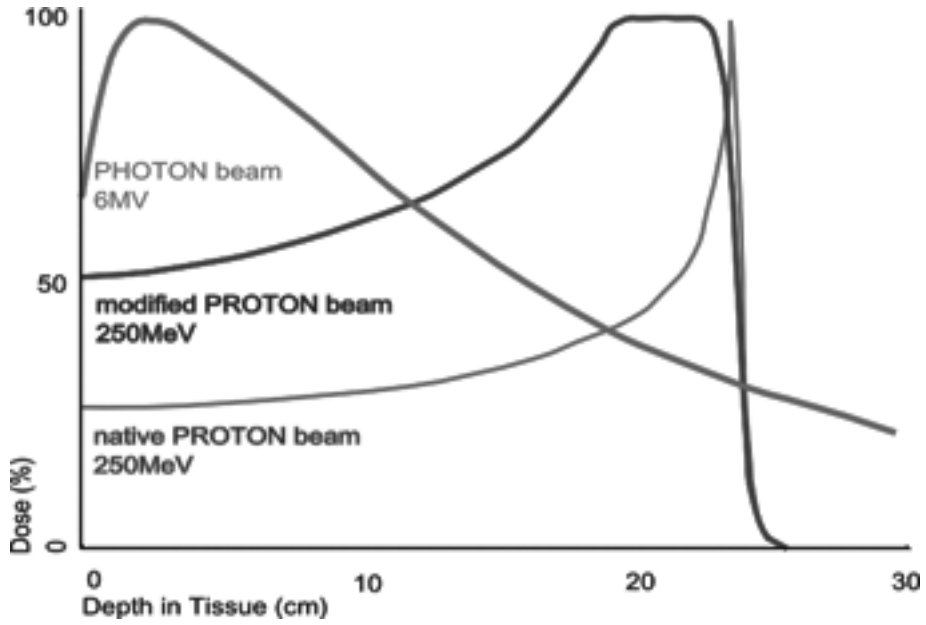

Figure 1.1: A comparison of photon and proton energy absorption in tissue. [3]

a strip entering the GTFE (GLAST Tracker Front End chip) into a pseudo-Gaussian via the shaper. The voltage in the shaper is compared to a threshold voltage via a discriminator and the amount of time that this voltage is larger than the threshold voltage is the TOT reading[4].

A modified version of the GLAST readout electronics has been developed at SCIPP to take data with the SSDs on a scale useful to the project and a Data Acquisition (DAQ) system based on the one developed for the Particle Tracking Silicon Microscope (PTSM)[5] at SCIPP is being employed to record the data. These images will be used by doctors to locate and measure tumors for accurate targeting during treatment.

1.3 Proton Energy Loss

The intent of these analyses is to measure the energy loss of protons as they pass through the SSDs and compare this measurement to theory. The theoretical model which applies in this case is the Bethe-Bloch equation, Eq. 1.1, which describes the energy loss per unit thickness dE/dx per

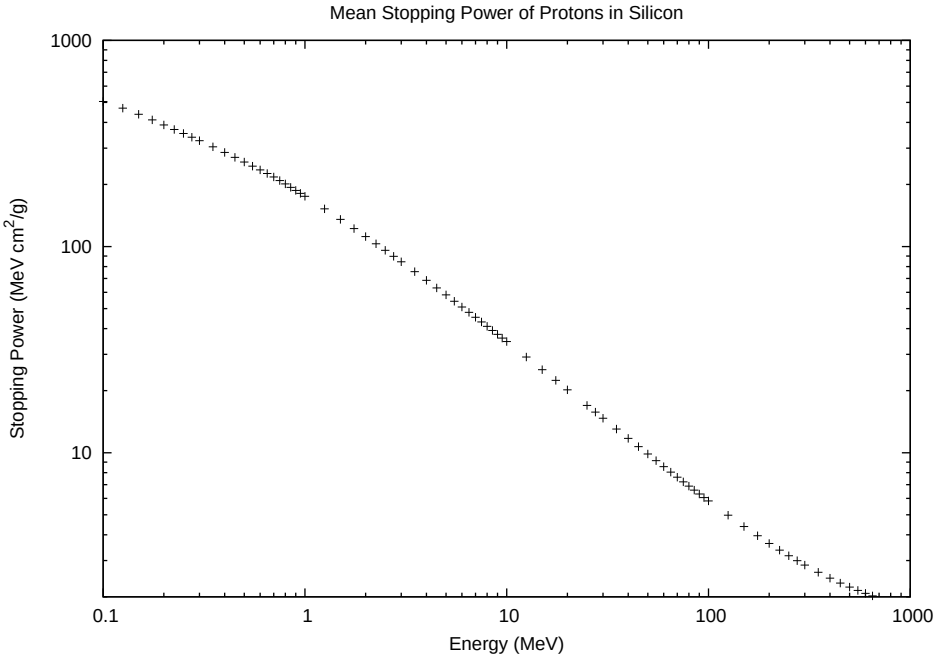

Figure 1.2: PSTAR stopping power data for Silicon. [7]

unit via the ionization of the atoms in a material[6]:

$$-\frac{dE}{dx} = Kz^2\frac{Z}{A}\frac{1}{\beta^2}\left[\frac{1}{2}\ln\frac{2m_ec^2\beta^2\gamma^2T_{max}}{I^2} - \beta^2 - \frac{\delta}{2}\right] \tag{1.1}$$

In this case, K/A $\approx 0.307\text{MeVg}^{-1}\text{cm}^2$, Z is the atomic number of the absorber, z is the charge of the incident particle in units of fundamental charge, β is the special relativistic $\frac{\text{v}}{\text{c}}$, $\text{m}_\text{e}\text{c}^2$ is $\approx$ 0.510MeV, γ is the Lorentz factor, T_max is the maximum kinetic energy which can be imparted to a free electron in a single collision (see below), and I is the mean excitation energy (10eV). T_max is described as the following:

$$T_{max} = \frac{2m_ec^2\beta^2\gamma^2}{1 + 2\gamma m_e/M + (m_e/M)^2} \tag{1.2}$$

where M is the incident particle mass (MeV/c^2). The National Institute of Standards and Technology (NIST) provides tables for the stopping powers, within 1 percent, of protons in different materials which include minor corrections to the Bethe-Bloch equation shown above.

With these data one can determine the total energy deposited within a material using the

integral $\Delta E = \int \frac{dE}{dx} dx$ or an equivalent small thickness approximation.

Table 1.1: Example data for relevant proton energies in Silicon.

Beam Energy (MeV)	Total Stopping Power ($MeVcm^2/g$)	Expected Energy Loss in 400μm Si (MeV)
3.50×10^{1}	1.302×10^{1}	1.21×10^{0}
1.00×10^{2}	5.838×10^{0}	5.44×10^{-1}
2.50×10^{2}	3.165×10^{0}	2.95×10^{-1}

2 Analysis

2.1 TOT analysis

At LLUMC The detector board was placed such that the tracking detectors were in the path of the proton beam. Tests were performed at various energies and readout configurations and data were collected. First, we see histograms of the TOT measurements from the SSDs for a beam energy of 250MeV (Fig. 2.1) at a threshold voltage of 103.5mV, internal triggering, and "ghosting" events (events for which multiple strips went over threshold that were not adjacent) removed for four different chip regions: The X plane (Layer 1) region and three regions on the Y plane (Layer 0); each corresponding to a pair of GTFEs that share a distinct shaping current. Increasing the current feeding the shaper by reducing the resistance in the circuit reduces the shaping time, the time it takes the shaper to reach a maximum voltage. Increasing the resistance, however, may cause the shaped pulse to be longer which may cause overflow in the TOT data. As we can see from Fig. 2.1 the MPV TOT increases inversely with shaper current (i.e. increases directly with shaper resistance) which is what we expect.

Next we see histograms of the TOT (Fig. 2.2 and 2.3) for energies 100MeV and 35MeV with similar results. An interesting thing to note is that as the incident particle energy decreases for a given region we see the MPV TOT increases which means that the amount of energy deposited increases which we know from Fig. (1.2). Also as particle energy decreases the amount of overflow, events for which measurement was higher than the maximum value, in the layer 1 increases from

$\approx$ 5% of total events to 9% and 20% for 250, 100, and 35MeV, respectively. At 35MeV in layer 0 region 1 (Fig. 2.3(b)) we can see that a large number of events are overflow. Also at 35MeV the histograms are considerably less smooth than their 100 and 250MeV counterparts. This may be explained by the Bethe-Bloch equation which shows that energy deposited by particles increases as their total energy decreases which means that the energies of particles passing through the detectors may become more varied as the initial beam energy decreases.

Because of the way the GTFEs work it is possible for more than one strip on the SSD to gain enough charge to go above threshold which we call a "cluster". When this happens, a single TOT is recorded: the largest value of TOT of all strips hit in an event. Because of this wider distribution of charge, we might expect to see a lower MPV TOT for a given beam energy as the number of strips in a cluster increases. What we do see, rather, is little or no difference in the mean TOT for varying cluster sizes. In fact, in some cases i.e. 250MeV beam energy (Fig. 2.4), we see the MPV TOT slightly increase suggesting more charge was deposited in the SSD. For 100MeV (Fig. 2.5) we do see a slight decrease in the MPV TOT as cluster size increases but the decrease is not significant. For 35MeV (Fig. 2.6) we do see a marked difference in MPV TOT for events with three strips over threshold but as the distribution bleeds into overflow, it is difficult to make a judgment on the significance of the increase.

If we look at the proportions of cluster sizes in Fig. 2.4(d), 2.6(d), and 2.5(d) we see a clear difference for 35MeV from 100 or 250MeV. The proportion of two and three strip events to single strip events increases noticeably. One possible explanation for this could be multiple Coulomb scattering which describes the scattering of nuclei as they pass close to other nuclei. The equation for the angle which encompasses 98% of the projected distribution is as follows[6]:

$$\theta_0 = \frac{13.6MeV}{\beta cp} z\sqrt{x/X_0}[1 + 0.038ln(x/X_0)] \tag{2.1}$$

According to Physics Letters B, "here, p, βc, and z are the momentum, velocity, and charge number of the incident particle, and x/X_0 is the thickness of the scattering medium in radiation lengths". In this case, z=1 for a proton, βc is 7.974×10^7m/s for a 35MeV proton, p is $8.621\times10^{-7}\frac{\text{MeV}*\text{s}}{\text{m}}$, and

x is the detector thickness of 400μm. X_0 is defined by the following equation:

$$X_0 = \frac{716.4\rho A}{Z(Z+1)ln(287/\sqrt{Z})} \tag{2.2}$$

which, since ρ=2.33g/cm^2, A=28 and Z=14 for silicon, gives us a value of 9.45cm. This means that θ_0 is 0.0102 radians. With a thickness of 400μm, θ_0 times the thickness will give us the approximate scattering length of 2.33μm. With a detector strip pitch, or distance between strips, of 228μm this means that multiple Coulomb scattering does not account for the increase of larger cluster sizes. An alternate explanation is that the increased energy deposition from lower energy particles is just enough to set strips that were otherwise charged for 100 and 250MeV beams over the threshold.

2.1.1 Figures

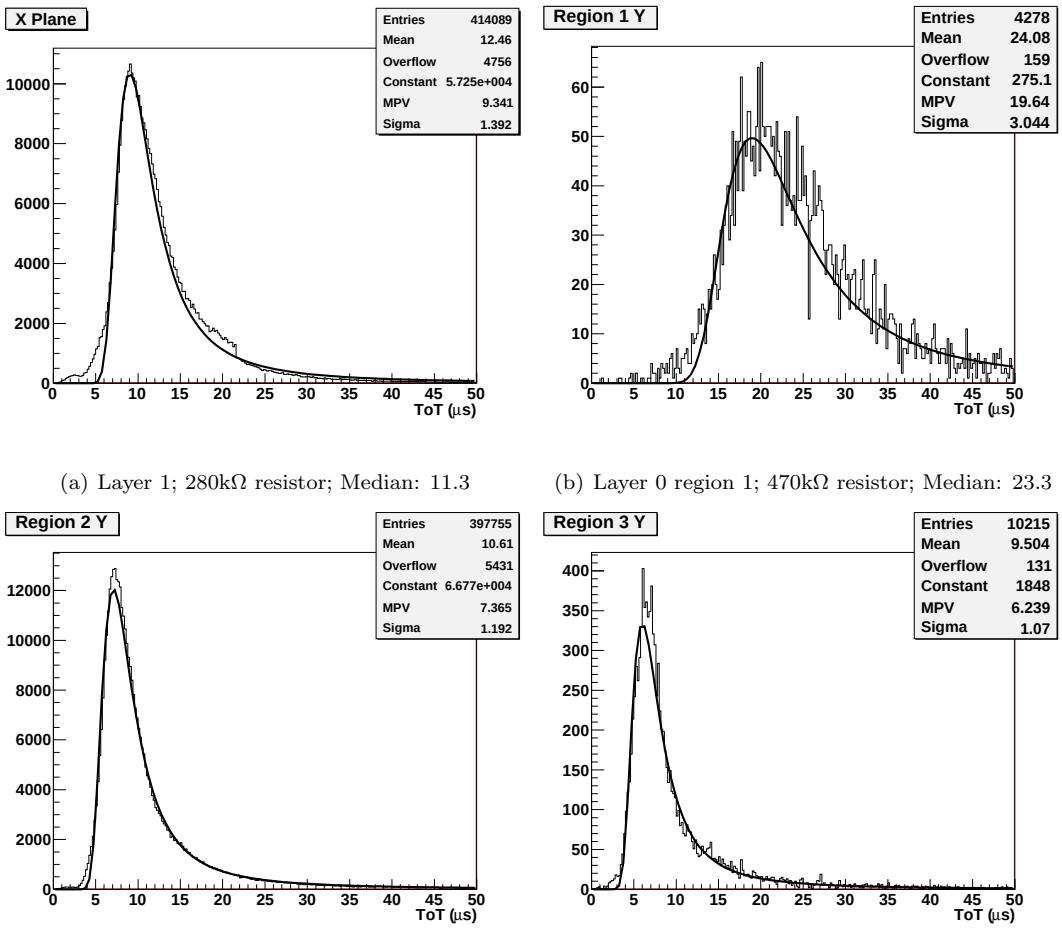

(a) Layer 1; 280kΩ resistor; Median: 11.3

(b) Layer 0 region 1; 470kΩ resistor; Median: 23.3

(c) Layer 0 region 2; 280kΩ resistor; Median: 8.9

(d) Layer 0 region 3; 180kΩ resistor: Median: 7.7

Figure 2.1: TOT histograms for all cluster sizes: 250MeV proton beam, 103.5mV threshold, all shaping resistors, internal triggering, ghosts removed

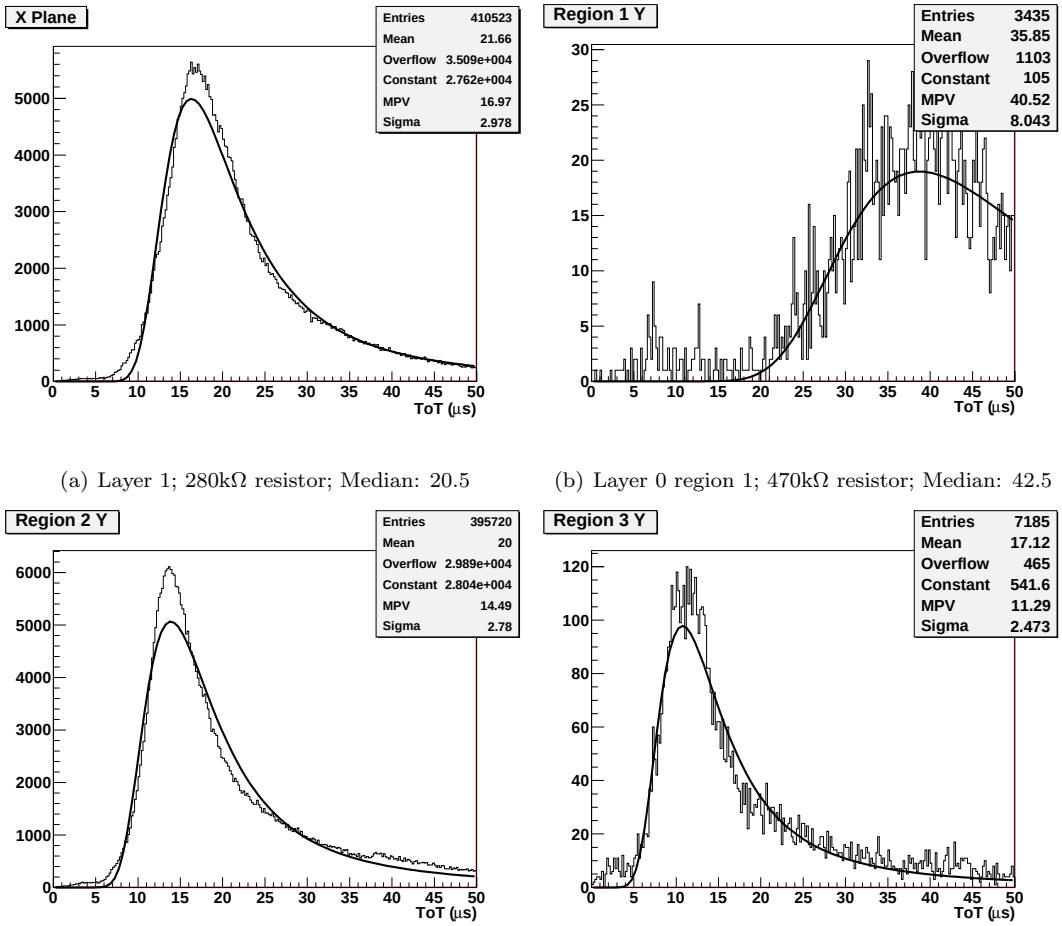

(a) Layer 1; 280kΩ resistor; Median: 20.5

(b) Layer 0 region 1; 470kΩ resistor; Median: 42.5

(c) Layer 0 region 2; 280kΩ resistor; Median: 17.9

(d) Layer 0 region 3; 180kΩ resistor; Median: 14.5

Figure 2.2: TOT histograms for all cluster sizes: 100MeV proton beam, 103.5mV threshold, all shaping currents, internal triggering, ghosts removed

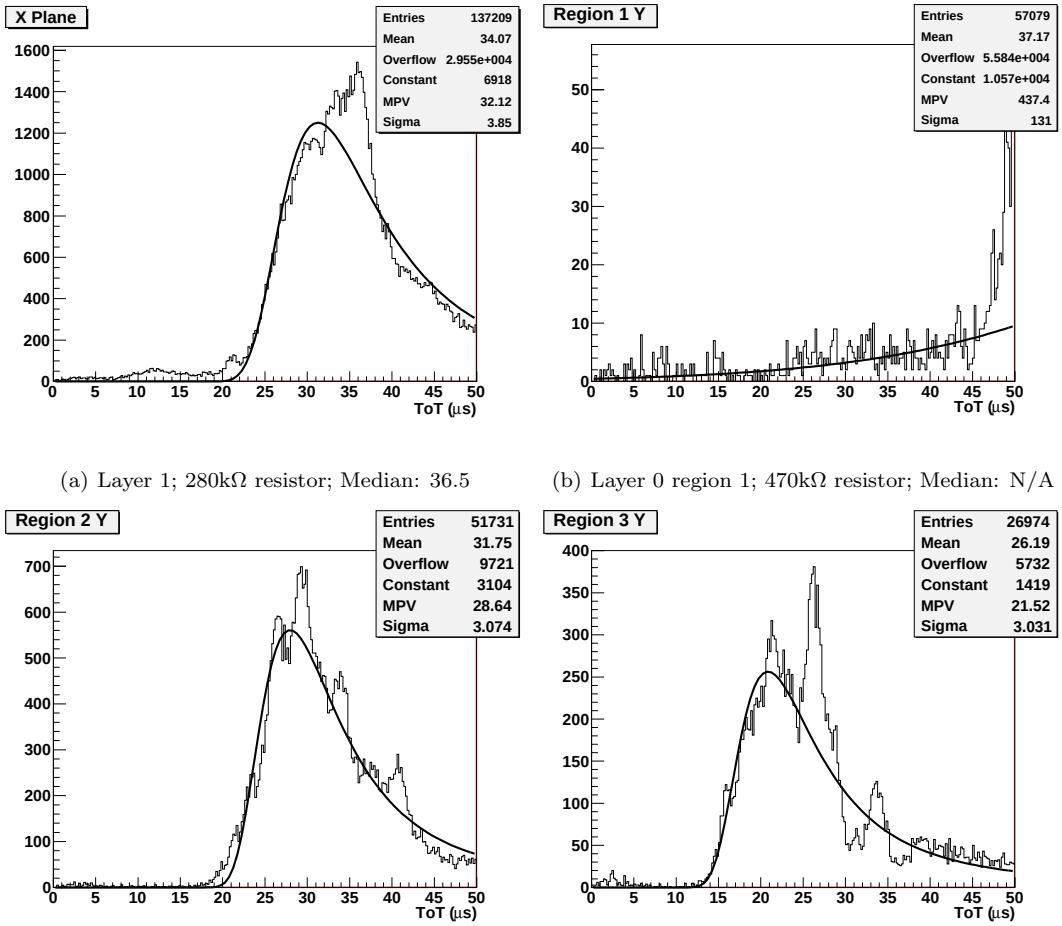

(a) Layer 1; 280kΩ resistor; Median: 36.5

(b) Layer 0 region 1; 470kΩ resistor; Median: N/A

(c) Layer 0 region 2; 280kΩ resistor; Median: 33.1

(d) Layer 0 region 3; 180kΩ resistor: Median: 27.1

Figure 2.3: TOT histograms for all cluster sizes: 35MeV beam energy, 103.5mV threshold, all shaping currents, internal triggering, ghosts removed

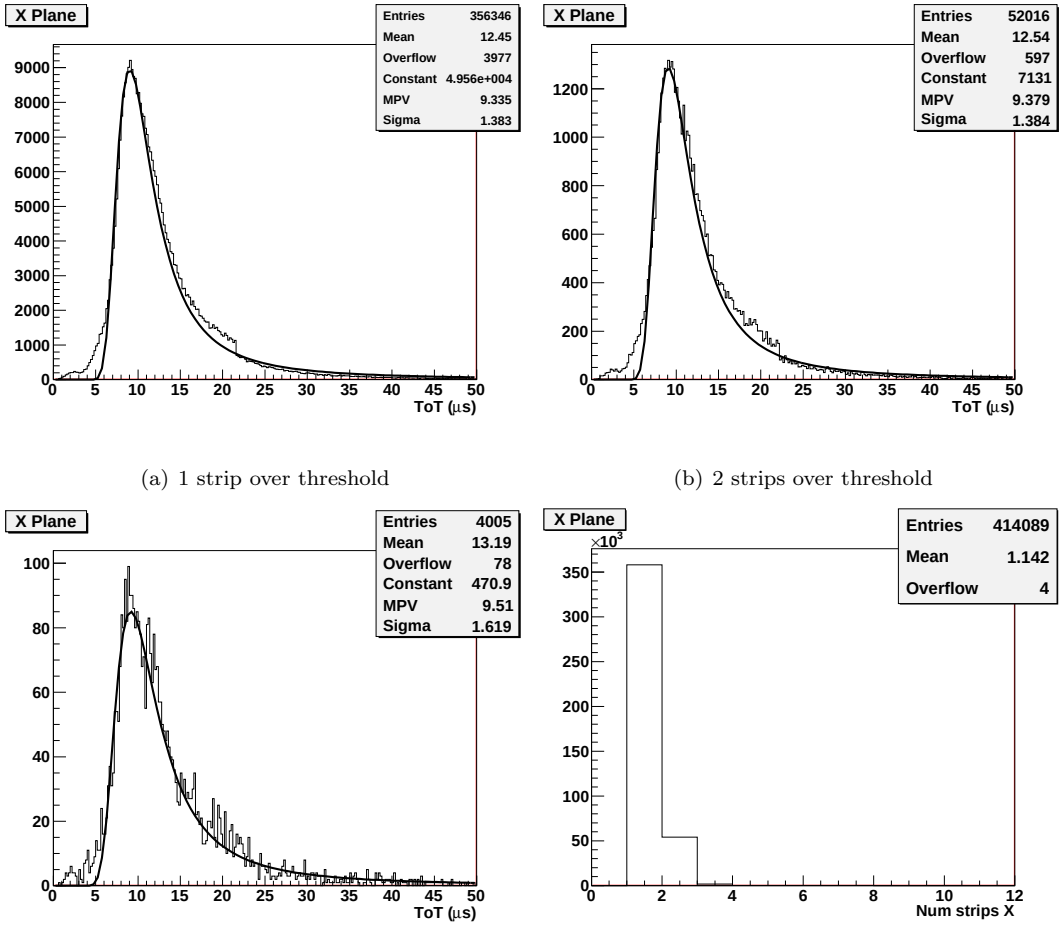

(a) 1 strip over threshold

(b) 2 strips over threshold

(c) 3 strips over threshold

(d) Cluster size

Figure 2.4: TOT histograms for varying cluster sizes: 250MeV beam energy, 103.5mV threshold, 280kΩ shaping resistor, internal triggering, ghosts removed

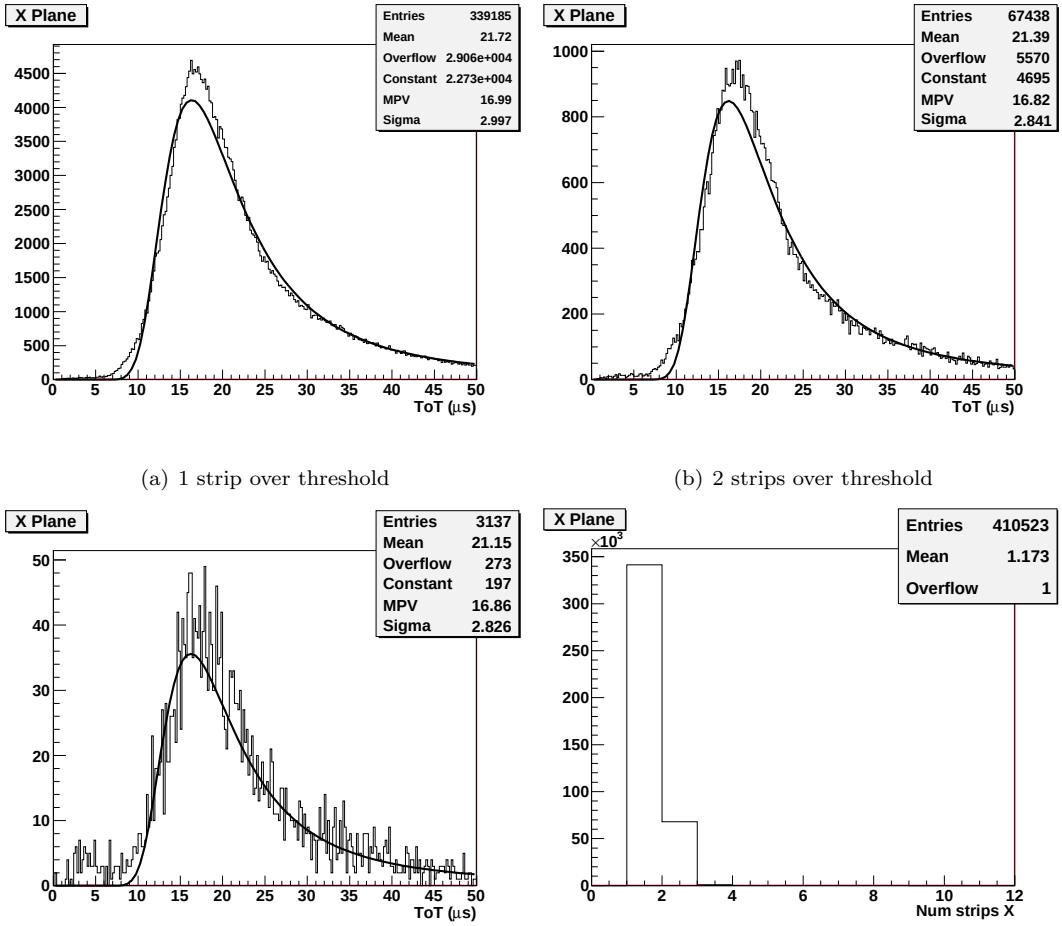

(a) 1 strip over threshold

(b) 2 strips over threshold

(c) 3 strips over threshold

(d) Cluster size

Figure 2.5: TOT histograms for varying cluster sizes: 100MeV beam energy, 103.5mV threshold, 280kΩ shaping resistor, internal triggering, ghosts removed

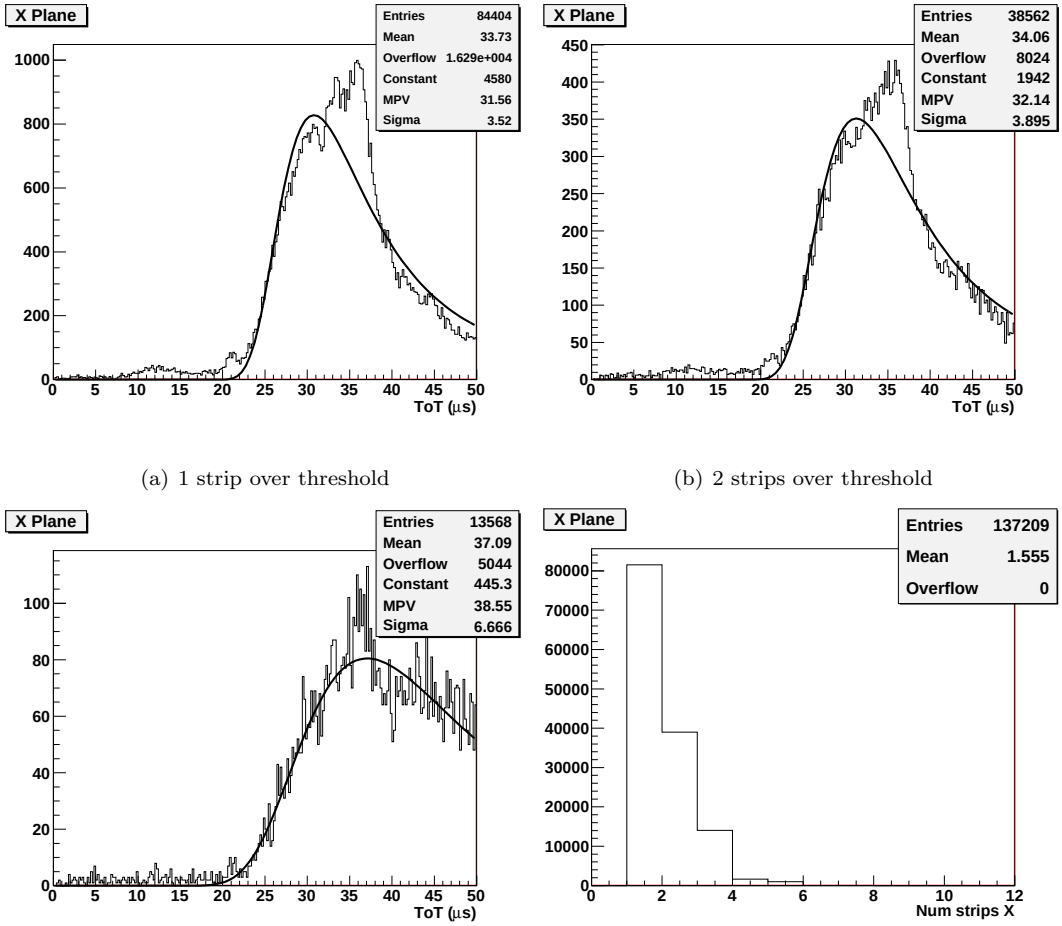

(a) 1 strip over threshold

(b) 2 strips over threshold

(c) 3 strips over threshold

(d) Cluster size

Figure 2.6: TOT histograms for varying cluster sizes: 35MeV beam energy, 103.5mV threshold, 280kΩ shaping resistor, internal triggering, ghosts removed

2.2 Energy loss of protons

To convert our TOT measurements into energy deposited we need to look at our TOT/Charge calibration data. Calibration takes place when a 46pF capacitor is charged with a known calibration voltage and the resulting charge is injected into a strip on the SSD. This creates a pulse within the GTFE's shaper which then gives us a TOT reading. With these data, we can create fits to correlate input charge with TOT, for a given threshold voltage, 103.5mV in this case.

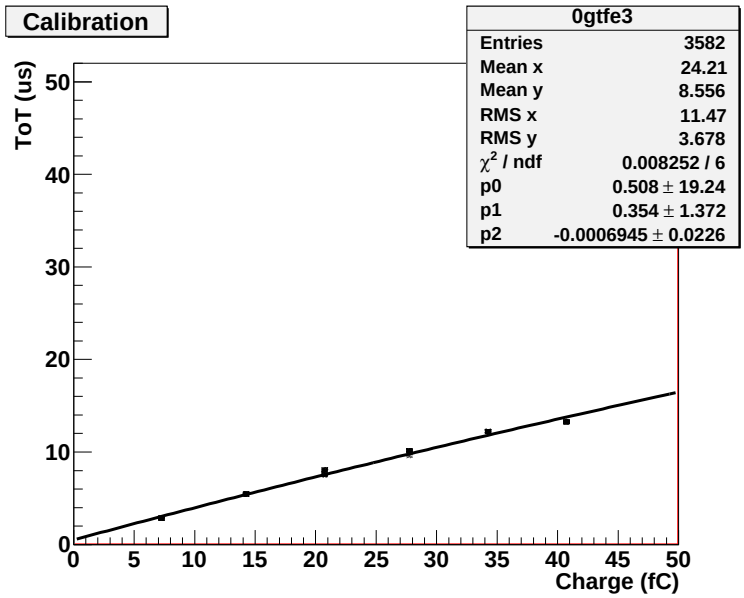

Figure 2.7: Layer 0, 280 $k\Omega$ calibration with second order approximation

As 2.7 shows, for example, we get a relationship for GTFE 3, Layer 0 that TOT $= -0.508 + 0.354\mathrm{Q} - 6.95\times10^{-4}\mathrm{Q}^2$. If we apply the mean TOT for a given beam energy to this formula, we can solve for Q and the lower root, on the ascending side of the quadratic, should be the value for the mean of the charge deposited in the detector. Because of the limitations of the calibration routine, calibration data plateaus at 25μs which is half of the maximum TOT the prototype can record. For beam test TOT data larger than 25μs the fits were extrapolated using the equations acquired from the calibration graphs which introduces a large amount of error for large TOTs.

Since using the mean, according to the histograms, isn't precise as there will always be

some overflow, we use the median, which is close to the mean (about 10% less than the mean in the case of Fig. 2.1(a)) and isn't affected by overflow, to estimate the real mean which will become more important for the cases with high overflow. This means that the calculations of the energy using the median will be an underestimate of the energy that could be calculated with the true mean.

When the charge is found, we can then convert it to energy using the following relationship:

$$\frac{\Delta E}{Q} = \frac{E_i}{e} \approx 0.02247 \frac{MeV}{fC} \tag{2.3}$$

where E is the energy deposited in MeV, Q is the charge deposited in fC, e is the elementary charge of an electron ($\approx 1.602\times10^{-4}$fC), and E_i is the energy required to create an electron-hole pair ($\approx 3.6\times10^{-6}$MeV). We can then compare this to the mean energy loss as outlined by NIST (Fig. 1.2) with the following equation:

$$\Delta E \approx \frac{dE}{dx}(MeVcm^2/g)\rho_{Si}\Delta x \tag{2.4}$$

where ρ_{Si} is the density of Silicon ($\approx 2.33\frac{g}{cm^3}$) and Δx is the detector thickness (.04cm). Since the mean energy deposited according to Eq. 2.4 at 100MeV is approximately 0.54MeV and the change in stopping power is less than 1% for this change in energy this is a good approximation for the energy deposited within 0.005MeV. Comparing this to the value of 1.24MeV we get from applying the median TOT of 17.9μs from table 2.1 to the calibration fit and Eq. 2.3 we see a difference experimental of 129% from the predicted value. Similarly the results of 0.56MeV and 2.71MeV we get for 250MeV and 35MeV beams differ from the expected values of 0.30MeV and 1.21MeV by 87% and 124% respectively. Table 2.1 and Fig. 2.11 show the results for the calculated mean energy loss along with the expected energy loss for various energies and shaping resistors.

If we compare the energies calculated between layer 1 and layer 0 region 2, we would expect to see very similar results as the energy lost when the beam passed through layer 0 would barely affect the energy loss in layer 1. Expected Energy Loss column of table 2.1 show, for example, 0.544MeV vs. 0.546MeV for a 100MeV beam for layers 0 and 1 respectively. What we see in fact is a substantial difference between the two results of 1.24MeV and 0.81MeV.

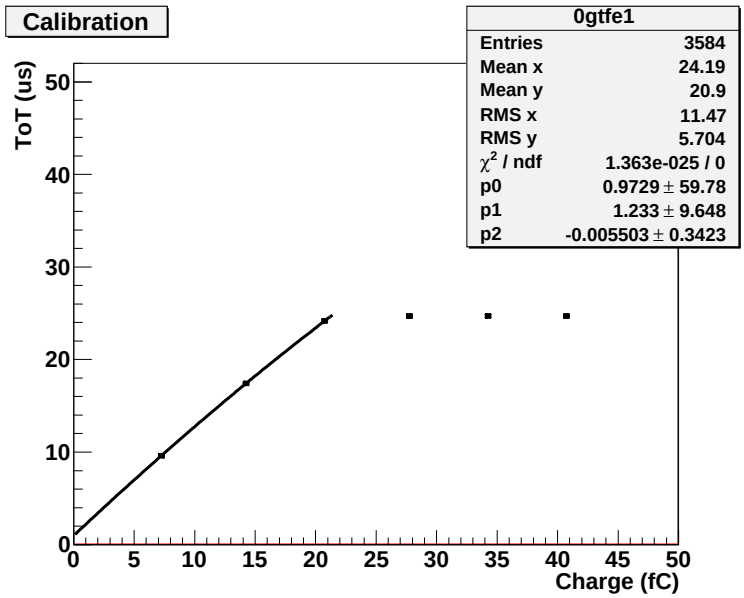

Figure 2.8: Layer 0, 470kΩ calibration with second order approximation up to 25μs

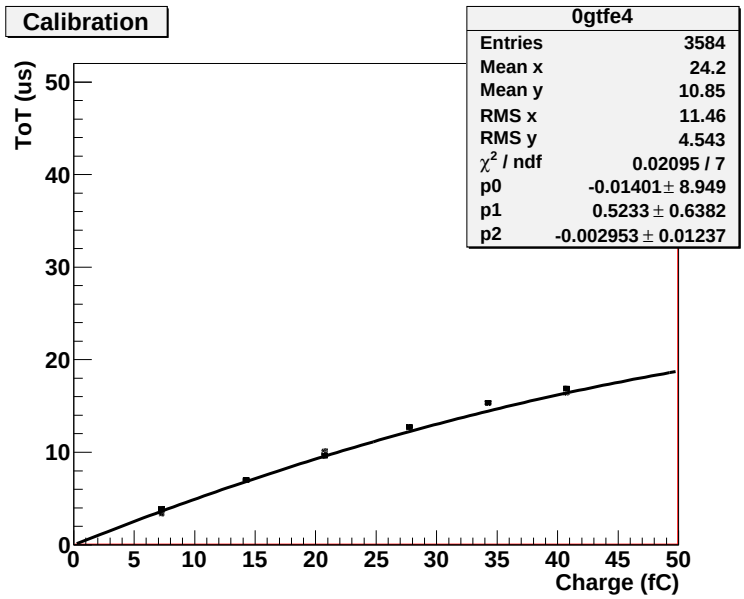

Figure 2.9: Layer 0, 180kΩ calibration with second order approximation

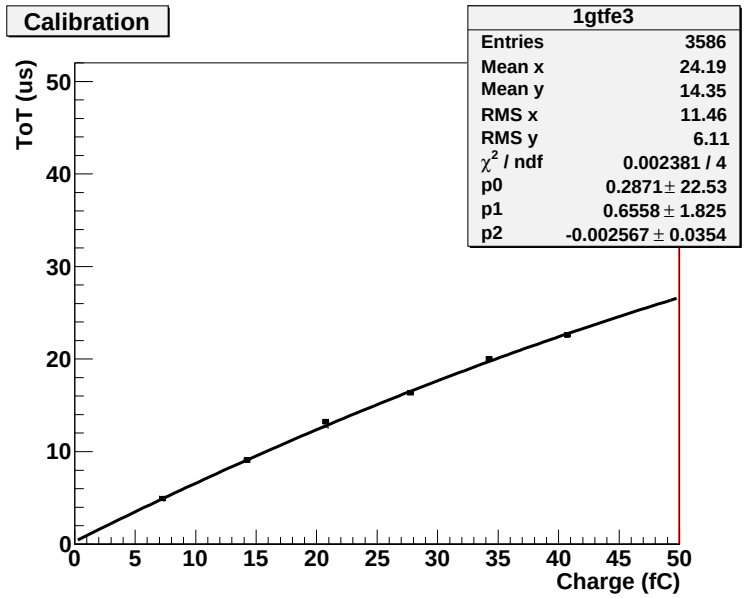

Figure 2.10: Layer 1, 280kΩ calibration with second order approximation

Table 2.1: Calculations for Energy Loss in Silicon

Beam Energy (MeV)	Layer	Shaping Resistor (kΩ)	Median TOT (μs)	Mean Charge Deposited (fC)	Mean Energy Loss (MeV)	Expected Energy Loss in 400μm Si (MeV)
	0	470	—	—†	—†	1.21
35	0	280	33.1	120.6	2.71	1.21
	1	280	36.5	80.7	1.81	1.25
	0	180	27.1	—†	—†	1.21
	0	470	42.5	41.3	0.93	0.54
100	0	280	17.9	55.1	1.24	0.54
	1	280	20.5	35.9	0.81	0.55
	0	180	14.5	34.4	0.77	0.54
	0	470	23.3	19.9	0.45	0.30
250	0	280	8.9	24.9	0.56	0.30
	1	280	11.3	18.1	0.41	0.30
	0	180	7.7	16.2	0.36	0.30

† TOT did not correspond to a charge according to calibration data fits.

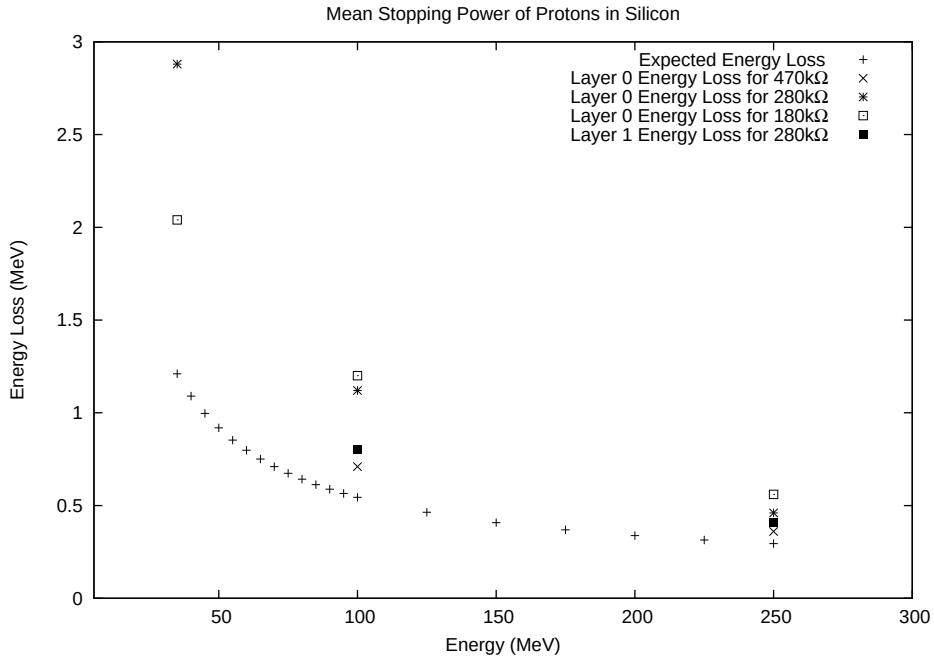

Figure 2.11: A plot of expected energy loss and calculated energy loss for all beam energies and shaper resistors.

3 Conclusions

Our findings show a 121%, 129%, and 87% discrepancy between the predicted and experimentally measured values of the energy deposited in the GLAST 2000 SSDs for proton beam energies of 35MeV, 100MeV, and 250MeV, respectively. This means that measuring the energy of the particle that was lost directly via the SSDs may not be an accurate method. An analysis of the energy detected by the calorimeter with and without the SSDs would show greater insight into the effects of the SSDs on the particles and thus the effectiveness of the SSDs in measuring energy.

Sources of error may include charge sharing between several strips or a different thickness of detector than assumed but as charge sharing would result in a lower TOT and therefore lower energy measured and the detectors should be close to the referenced thickness within less than 1μm these sources are unlikely and would have little effect anyway.

Bibliography

[1] Loma Linda University Medical Center. "Proton Technology." 17 Jun 2009 <http://www.protons.com/proton-therapy/proton-technology.html>.

[2] W. P. Levin, "Proton beam therapy." *British Journal of Cancer*, 93.849854, 27 Sep 2005.

[3] Wikipedia. "Bragg Peak." 17 Jun 2009 <http://en.wikipedia.org/wiki/File:BraggPeak.png>.

[4] R. Johnson, "Tracker Front End Readout ASIC Specification." LAT-SS-00169-4, 3 Mar 2003, pp. 9, 10.

[5] B. Keeney, "The Design, Implementation, And Characterization Of A Prototype Readout System For The Particle Tracking Silicon Microscope." (M.S. Thesis) University of California Santa Cruz, Sep 2004.

[6] L. Alvarez-Gaumé, "Review of Particle Physics." *Physics Letters B. Elsevier*, 592.1-4, 15 Jul 2004, pp. 242-245.

[7] National Institute of Standards and Technology. "PSTAR." 17 Jun 2009 <http://physics.nist.gov/PhysRefData/Star/Text/PSTAR.html>.